

RESIDUAL DENSE SWIN TRANSFORMER FOR CONTINUOUS DEPTH-INDEPENDENT ULTRASOUND IMAGING

Jintong Hu, Hui Che, Zishuo Li, Wenming Yang[†]

Tsinghua Shenzhen International Graduate School, Tsinghua University

ABSTRACT

Ultrasound imaging is crucial for evaluating organ morphology and function, yet depth adjustment can degrade image quality and field-of-view, presenting a depth-dependent dilemma. Traditional interpolation-based zoom-in techniques often sacrifice detail and introduce artifacts. Motivated by the potential of arbitrary-scale super-resolution to naturally address these inherent challenges, we present the Residual Dense Swin Transformer Network (RDSTN), designed to capture the non-local characteristics and long-range dependencies intrinsic to ultrasound images. It comprises a linear embedding module for feature enhancement, an encoder with shifted-window attention for modeling non-locality, and an MLP decoder for continuous detail reconstruction. This strategy streamlines balancing image quality and field-of-view, which offers superior textures over traditional methods. Experimentally, RDSTN outperforms existing approaches while requiring fewer parameters. In conclusion, RDSTN shows promising potential for ultrasound image enhancement by overcoming the limitations of conventional interpolation-based methods and achieving depth-independent imaging.

Index Terms— Ultrasound imaging, Arbitrary-scale image super-resolution, Depth-independent imaging, Non-local implicit representation

1. INTRODUCTION

Ultrasound imaging serves as a pivotal tool in medical diagnostics for its non-invasive nature and real-time imaging capabilities, allowing visualization of superficial and deep structures [1]. However, adjusting the imaging depth presents challenges that impact image quality and field-of-view [2].

Modifying the imaging depth in ultrasound requires altering the echo reception time. Longer reception times, necessary for deeper imaging, tend to lower the frame rate, subsequently reducing temporal resolution [3]. A shallow imaging depth, however, may lead to interference from adjacent echo

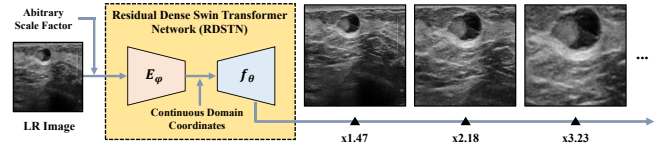


Fig. 1. An example of magnified images of arbitrary scales generated by RDSTN.

signals, compromising image quality. Therefore, selecting the appropriate depth threshold is crucial.

Traditionally, zoom-in operations utilizing interpolation have been employed to counterbalance unsatisfactory image quality during depth adjustments [4]. This often results in the loss of intricate details and the emergence of aliasing artifacts.

Addressing this challenge, our study presents the arbitrary-scale super-resolution (ASSR) as a cutting-edge approach that offers an effective solution within the desired depth threshold. Existing ASSR models often overlook the unique attributes of datasets, a particularly critical aspect given the notable long-range similarities in ultrasound images.

To address the shortcoming, we introduce the Residual Dense Swin Transformer Network (RDSTN), which integrates a linear embedding layer, a Residual Dense Shifted-window Transformer (RDST) encoder, and a Multilayer Perceptron (MLP) decoder. The linear embedding layer projects the input into higher-dimensional space for enhanced feature extraction. The RDST encoder leverages non-locality to promote essential feature reuse. Finally, the MLP decoder maps each target pixel coordinate to its corresponding latent code, achieving refined reconstruction of detail. Figure 1 shows an example of magnified images generated by RDSTN.

In conclusion, our contributions are:

- The first introduction of implicit neural representation-based arbitrary-scale super-resolution to multiple organ ultrasound datasets, ensuring a versatile and depth-independent display.
- Proposing an efficient non-local encoder to model the spatial dependencies between pixels, reducing parameters by 45% with respect to the state-of-the-art method.
- Conducting extensive experiments to prove the capability of RDSTN in addressing the balance issue.

[†]This work was partly supported by the National Natural Science Foundation of China (Nos.62171251&62311530100) and the Special Foundations for the Development of Strategic Emerging Industries of Shenzhen (Nos.JSGG20211108092812020&CJGJZD20210408092804011).

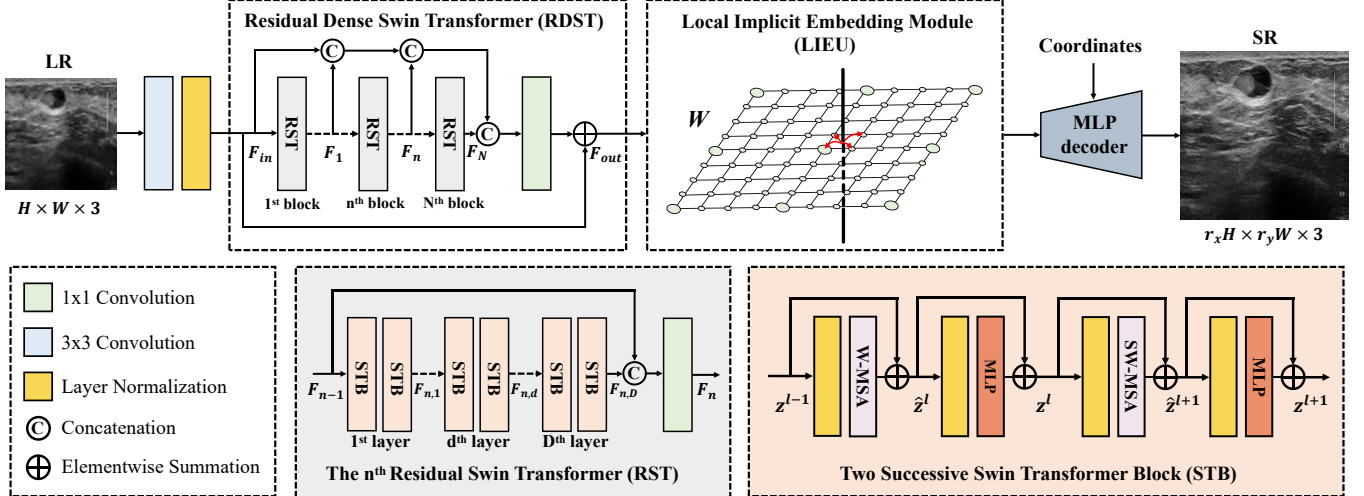


Fig. 2. The main pipeline of our RDSTN. RDSTN introduces non-locality and allows for essential feature reuse, improving representation and performance.

2. RELATED METHODS

2.1. Single Image Super-Resolution

Numerous single image super-resolution (SISR) methods have been proposed over time. Among the earlier techniques, interpolation stands out, which works by filling values between pixels to enhance image resolution. However, its major downside is the inability to restore intricate details effectively. Recently, deep learning-based methods have taken the spotlight in the SISR domain. Notably, Convolutional Neural Networks (CNNs) are now widely recognized due to their prowess in autonomously learning hierarchical features and establishing a relationship between low-resolution (LR) and high-resolution (HR) images. The SRCNN [5], a notable CNN-based model, leverages a three-layer CNN structure to learn this LR to HR mapping. Various other models, such as VDSR [6], EDSR [7], ESPCN [8], LapSRN [9], MemNet [10], RDN [11], and DBPN [12], have carved their niche by adopting unique strategies. These include deep architectures, sub-pixel convolutional layers, the Laplacian pyramid framework, memory blocks, cascaded ResNet-like blocks, densely connected residual blocks, and deep back-projection units. However, a common limitation across these models is their lack of flexibility due to predefined upsampling mechanisms, thereby confining their application to fixed integer-scale super-resolution.

2.2. Arbitrary-Scale Image Super-Resolution

Arbitrary-scale super-resolution (ASSR) techniques are gaining traction due to their adaptability in handling super-resolution tasks across various scaling factors [13–19]. MetaSR [15] led the charge in CNN-based methods for ASSR, while

LIIF [16] showcased an innovative framework by leveraging implicit neural representations to treat images as continuous functions. Specifically, LIIF uses a Multi-Layer Perceptron (MLP) to determine RGB values from feature maps, coordinates, and scaling factors. Building on the foundation set by LIIF, other ASSR studies have emerged. For instance, LTE [17] inputs coordinates into a high-dimensional Fourier feature space to tackle spectral bias. SADN [18] augments the latent code drawn by the encoder with multi-scale features. A-LIIF [19] addresses artifacts by capturing pixel differences using multiple MLPs. Nevertheless, a limitation of these methods is their dependence on convolution or fully connected layers, which curtails the encoder’s capacity to glean global information and might bypass crucial spatial similarities among pixels. Consequently, integrating non-locality into the encoder is imperative.

3. MODEL ARCHITECTURE

This section introduces the proposed Residual dense swin transformer network (RDSTN). The main pipeline of our RDSTN is shown in Figure 2.

3.1. Residual Dense Swin Transformer Encoder

Swin Transformer block [22] has emerged as a highly promising architecture due to its unique capabilities in handling computation cost and non-local characteristics. Our proposed Residual Dense Swin Transformer (RDST) encoder is designed on the basis of swin transformer block, composed of four hierarchical stages, each with six consecutive swin transformer blocks. The output of each stage maintains a fixed resolution and number of channels, thus the latent codes extracted by RDST have the same spatial resolution as the LR

Table 1. Quantitative comparison in terms of PSNR(dB). The evaluation is performed on the BUSI testing set. The models are trained with continuous scale sampled from $U(1, 4)$. Best result of each scale is in bold.

Methods	Num. of Parameters	In-distribution							Out-distribution		
		×1.6	×1.7	×1.8	×1.9	×2	×3	×4	×6	×8	×10
Bicubic	–	40.21	39.36	38.88	38.21	38.68	33.17	30.40	26.88	24.86	23.64
EDSR-LIIF [16]	496.4K	43.92	43.06	42.26	41.50	40.80	35.80	32.87	29.42	27.34	26.04
RDN-LIIF [16]	5.8M	44.71	43.81	43.03	42.28	41.57	36.36	33.22	29.58	27.46	26.12
Unet [20]	31.4M	42.39	41.71	41.05	40.42	39.83	35.24	32.55	29.20	27.16	25.91
Resnet50 [21]	4.1M	42.86	42.07	41.35	40.62	39.95	35.17	32.46	29.12	27.11	25.87
RDSTN (ours)	3.2M	44.78	43.89	43.10	42.35	41.62	36.34	33.20	29.64	27.54	26.18

Table 2. Ablation study of RDSTN on Local Feature Fusion (LFF) and Global Feature Fusion (GFF). The evaluation is performed on the BUSI testing set, with a focus on measuring the peak signal-to-noise ratio (PSNR(dB)) to assess the performance of these strategies. The best result of each scale is in bold.

Model Settings	Module		In-distribution							Out-distribution		
	LFF	GFF	×1.2	×1.4	×1.6	×1.8	×2	×3	×4	×6	×8	×10
S_1	✗	✗	48.65	46.17	44.36	42.69	41.21	36.04	33.01	29.51	27.42	26.07
S_2	✗	✓	48.71	46.23	44.42	42.73	41.27	36.07	33.03	29.54	27.46	26.11
S_3	✓	✗	48.89	46.40	44.61	42.94	41.46	36.23	33.13	29.59	27.50	26.14
S_4	✓	✓	49.27	46.62	44.78	43.10	41.62	36.34	33.20	29.64	27.54	26.18

counterparts. Therefore, every pixel in low-resolution images can match a latent code in the same position. RDST assists the model to extract non-locality in broader receptive fields at the beginning stages, while retaining fine-grained detail at the higher stages.

A distinctive innovation in RDST is the fusion of both local and global features, enabling the model to retain vital contextual information throughout its processing stages. This is achieved by adeptly concatenating outputs from each stage, thereby harnessing the rich feature spectrum across varying layers and blocks. To foster rapid model convergence, we incorporate residual connections with the originating image. Additionally, RDST adopts a cyclic interplay among successive layers, a strategic maneuver ensuring that the all-encompassing non-local information is captured with refined precision.

Specifically, global feature fusion and local feature fusion can be formulated as:

$$F_{out} = F_{in} + Conv_{1 \times 1}([F_{in}, F_1, \dots, F_N]) \quad (1)$$

$$F_n = Conv_{1 \times 1}([F_{n-1}, STB^D(F_{n-1})]) \quad (2)$$

where STB denotes the swin transformer blocks. F_i denotes the output of the i^{th} RST block ($i \in 1, \dots, N$). $Conv_{1 \times 1}$ represents the convolution operation with 1×1 kernel size, which is used to recover channels.

3.2. Local Enhanced Implicit Representation Upscaling

Building on the paradigm of LIIF [16], we introduce the Local Enhanced Implicit Representation Upscaling (LEIRU) decoder. This refined Multi-Layer Perceptron (MLP) is tailored

to operate on the coordinates of the anticipated scale super-resolution image, aligning each coordinate with its nearest latent code. For a singular coordinate, denoted as x_q , its corresponding nearest latent code is represented as $C(x_q)$. The RGB values for every coordinate are thus defined by:

$$RGB(x_q) = MLP([C(x_q), x_q - x^*]) \quad (3)$$

where MLP represents an MLP with learnable parameters, x^* denotes the coordinate of $C(x_q)$.

In essence, the relative distance gauges the affinity between features and latent codes. A closer coordinate to the latent code implies higher similarity, gauged by the inverse of this relative distance. The underlying premise is that coordinates within the same grid derive from the same latent code, thereby utilizing local information. The non-local encoder’s design is pivotal to infuse non-locality into the local decoder, optimizing the model’s performance.

However, an issue arises when a coordinate traverses the grid boundary. At this juncture, the MLP output can shift dramatically due to the abrupt latent code alteration, resulting in chessboard artifacts in the output image. To mitigate this, our module introduces a local ensemble operation. Drawing from interpolation principles, the local ensemble harnesses the weights of the rectangle, formed by the coordinate and its four adjacent latent codes, executing a nearest neighbor interpolation. Mathematically, this is articulated as:

$$LEIRU(x_q) = \sum_{x_i \in grid} w_{x_i} RGB(x_i) \quad (4)$$

where w_{x_i} represents the weights for each coordinate x_i . $RGB(x_i)$ represents the corresponding RGB values computed by the MLP for the coordinate x_i .

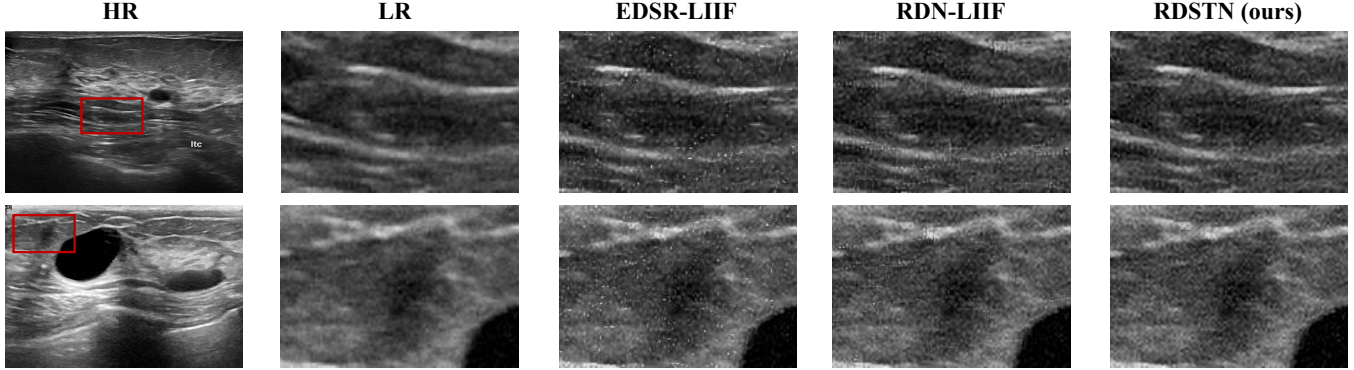


Fig. 3. Visual comparison between methods. RDSTN achieves better continuity in texture and has the fewest white noise points compared to other methods.

4. EXPERIMENT RESULTS

We utilize the BUSI dataset [23], which comprises 779 high-resolution breast ultrasound images, to train our model. We allocate 80% of these images for training, with the remainder designated for testing. In line with prior research, our primary evaluation metric is the peak signal-to-noise ratio (PSNR).

4.1. Comparison with other methods

We benchmark our RDSTN against other implicit representation techniques, such as EDSR-LIIF, RDN-LIIF [16], and the conventional bicubic interpolation [24]. Table 1 showcases the qualitative results. Across various scales, both within and beyond distribution, our method surpasses contemporary techniques while utilizing fewer parameters. When tested on low-resolution images tainted with Gaussian noise, the visual evidence in Figure 3 reveals our method’s superiority in minimizing white noise spots and maintaining texture continuity. Therefore, our approach not only excels in standard metrics but also demonstrates impressive noise resistance.

4.2. Ablation Study

To further validate the efficacy of our model, we perform an ablation study on global and local feature fusion strategies. Our experiments indicate that setting S_4 yields the best results among all the tested scales, followed by S_3 , S_2 , and S_1 , respectively. This underscores the effectiveness of our designed local and global feature fusion, with detailed results provided in Table 2. By integrating both global and local feature fusion, our network enhances its ability to capture non-local features while simultaneously reducing computational costs.

4.3. Generalization

To further assess the generalization capability of our model, we train it on breast ultrasound images and subsequently test on different tissues, including thyroid and carotid arteries.

Table 3. Generalization test of RDSTN on out-distribution dataset. The evaluation is performed on the 2023 MICCAI ultrasound enhancement challenge dataset, we use PSNR(dB) to assess the performance. The best result is in bold.

Method	scale				
	×1.6	×1.7	×1.8	×1.9	×2
train: BUSI [23], test: MICCAI USenhance breast					
Bicubic	34.28	33.52	31.55	31.23	31.66
EDSR-LIIF	35.30	34.55	33.63	33.07	32.42
RDN-LIIF	35.12	34.41	33.56	33.13	32.47
RDSTN (ours)	35.35	34.62	33.74	33.23	32.59
train: BUSI [23], test: MICCAI USenhance thyroid					
Bicubic	38.17	37.14	34.91	34.26	34.81
EDSR-LIIF	39.87	38.73	37.72	36.86	36.07
RDN-LIIF	39.91	38.77	37.76	36.90	36.10
RDSTN (ours)	39.99	38.81	37.83	36.96	36.14
train: BUSI [23], test: MICCAI USenhance carotid					
Bicubic	38.11	37.14	34.95	34.37	34.84
EDSR-LIIF	40.05	38.96	37.90	37.07	36.21
RDN-LIIF	40.08	38.98	37.89	37.11	36.28
RDSTN (ours)	40.16	39.07	37.99	37.17	36.30

The results, present in Table 3, show that our model surpasses other methods, highlighting its strong generalization potential. Thus, our model can deliver exceptional results on expansive samples even when trained on a small, focused dataset, underscoring its adaptability in practical applications.

5. CONCLUSION

Our advanced RDSTN effectively tackles the challenges associated with long-range modeling and non-local feature extraction in arbitrary-scale super-resolution. It streamlines the delicate balance between image quality and field-of-view, showcasing enhanced noise suppression capabilities. Testing reveals that RDSTN performs competitively in both metrics and visual quality compared to other methods, yet utilizes fewer parameters. Through RDSTN, we can adeptly navigate continuous imaging at suitable depth thresholds.

6. ACKNOWLEDGMENTS

We wish to extend our heartfelt appreciation to the organizers of the 2023 Ultrasound Image Enhancement (USenhance) Challenge for availing the dataset pivotal for our generalization examination. Dataset can be accessed via the official 2023 USenhance portal: <https://ultrasoundenhance2023.grandchallenge.org/>.

References

- [1] Carmel M. Moran and Adrian J. W. Thomson, “Pre-clinical ultrasound imaging—a review of techniques and imaging applications,” *Frontiers in Physics*, vol. 8, 2020.
- [2] Giner Maslebu, Kusworo Adi, and Suryono, “Effect of gain changing to maximum visualization depth on diagnostic ultrasound b-mode image,” *International Journal of Applied Engineering Research*, vol. 10, pp. 33449–33452, 08 2015.
- [3] Gowthaman Gunabushanam and Leslie M. Scutt, “Ultrasound image optimization for the interventional radiologist,” *Techniques in Vascular and Interventional Radiology*, vol. 24, no. 3, pp. 100766, 2021.
- [4] Zander D, Hüske S, Hoffmann B, Cui XW, Dong Y, Lim A, Jenssen C, Löwe A, Koch JBH, and Dietrich CF, “Ultrasound image optimization (“knobology”): B-mode,” *Ultrasound Int Open*, vol. 6, no. 1, 08 2020.
- [5] Chao Dong, Chen Change Loy, Kaiming He, and Xiaou Tang, “Image super-resolution using deep convolutional networks,” 2015.
- [6] Jiwon Kim, Jung Kwon Lee, and Kyoung Mu Lee, “Accurate image super-resolution using very deep convolutional networks,” 2016.
- [7] Bee Lim, Sanghyun Son, Heewon Kim, Seungjun Nah, and Kyoung Mu Lee, “Enhanced deep residual networks for single image super-resolution,” 2017.
- [8] Wenzhe Shi, Jose Caballero, Ferenc Huszár, Johannes Totz, Andrew P. Aitken, Rob Bishop, Daniel Rueckert, and Zehan Wang, “Real-time single image and video super-resolution using an efficient sub-pixel convolutional neural network,” 2016.
- [9] Wei-Sheng Lai, Jia-Bin Huang, Narendra Ahuja, and Ming-Hsuan Yang, “Deep laplacian pyramid networks for fast and accurate super-resolution,” 2017.
- [10] Ying Tai, Jian Yang, Xiaoming Liu, and Chunyan Xu, “Memnet: A persistent memory network for image restoration,” 2017.
- [11] Yulun Zhang, Yapeng Tian, Yu Kong, Bineng Zhong, and Yun Fu, “Residual dense network for image super-resolution,” 2018.
- [12] Muhammad Haris, Greg Shakhnarovich, and Norimichi Ukita, “Deep back-projection networks for super-resolution,” 2018.
- [13] Xintao Wang, Ke Yu, Chao Dong, and Chen Change Loy, “Recovering realistic texture in image super-resolution by deep spatial feature transform,” in *2018 IEEE/CVF Conference on Computer Vision and Pattern Recognition*, 2018, pp. 606–615.
- [14] Tamar Rott Shaham, Tali Dekel, and Tomer Michaeli, “Singan: Learning a generative model from a single natural image,” in *2019 IEEE/CVF International Conference on Computer Vision (ICCV)*, 2019, pp. 4569–4579.
- [15] Xuecai Hu, Haoyuan Mu, Xiangyu Zhang, Zilei Wang, Tieniu Tan, and Jian Sun, “Meta-sr: A magnification-arbitrary network for super-resolution,” 2019.
- [16] Yinbo Chen, Sifei Liu, and Xiaolong Wang, “Learning continuous image representation with local implicit image function,” 2021.
- [17] Jaewon Lee and Kyong Hwan Jin, “Local texture estimator for implicit representation function,” 2022.
- [18] Hanlin Wu, Ning Ni, and Libao Zhang, “Scale-aware dynamic network for continuous-scale super-resolution,” 2021.
- [19] Hongwei Li, Tao Dai, Yiming Li, Xueyi Zou, and Shu-Tao Xia, “Adaptive local implicit image function for arbitrary-scale super-resolution,” 2022.
- [20] Olaf Ronneberger, Philipp Fischer, and Thomas Brox, “U-net: Convolutional networks for biomedical image segmentation,” 2015.
- [21] Kaiming He, Xiangyu Zhang, Shaoqing Ren, and Jian Sun, “Deep residual learning for image recognition,” 2015.
- [22] Ze Liu, Yutong Lin, Yue Cao, Han Hu, Yixuan Wei, Zheng Zhang, Stephen Lin, and Baining Guo, “Swin transformer: Hierarchical vision transformer using shifted windows,” 2021.
- [23] Walid Al-Dhabyani, Mohammed Gomaa, Hussien Khaled, and Aly Fahmy, “Dataset of breast ultrasound images,” *Data in Brief*, vol. 28, pp. 104863, 2020.
- [24] R. Keys, “Cubic convolution interpolation for digital image processing,” *IEEE Transactions on Acoustics, Speech, and Signal Processing*, vol. 29, no. 6, pp. 1153–1160, 1981.